STRUCTURAL BEHAVIOR OF THIN-WALLED, PRETWISTED COMPOSITE BLADES WITH MULTI-CELL SECTIONS

Sung Nam Jung,* and Il-Ju Park†
Department of Aerospace Engineering
Chonbuk National University, Jeonju 561-756, South Korea

Abstract

In this work, a mixed beam approach is performed for the structural response of thin-walled, multi-celled composite blades with built-in twist. The analytical model includes the effects of elastic couplings, shell wall thickness, and torsion warping. The Reissner's semi-complimentary energy functional is used to derive the beam force-displacement relations. The bending and torsion-related warpings introduced by the pretwist effect are derived in a closed form in the beam formulation. An extensive validation study has been carried out to correlate the current analysis with available literature and detailed finite element structural analysis results. Various cross-section blades are considered in the comparison study. These include pretwisted beams with rectangular solid and single-cell box section, composite beams with two-cell box section, and two-celled composite blades with extension-torsion couplings. Very good correlation has been obtained for cases considered. The effects of pretwist and fiber orientation angles on the static behavior of thin-walled composite beams with multi-cell sections are also investigated.

Introduction

During the past couple of decades, pretwisted blades have attracted a lot of attention especially for helicopters, propellers, tilt rotors, and wind turbine applications. In a structural point of view, the pretwist affects not only on the torsional property but also on the bending rigidity. Besides this direct characteristic, the pretwist introduces a coupling between extension and torsion, even for blades with isotropic materials. For the composite case, there will be an additional coupling between bending and shear. It is apparent that these structural couplings make the analysis more involved than that without the pretwist effect especially with composite materials.

Rosen [1] presented an extensive review dealing with statics, dynamics, and stability aspects of pretwisted beams. It is suggested that the appropriate treatment of section warpings (e.g., torsion warping) is viable for refined structural analysis of pretwisted blades. In addition, bending-related warpings as well as torsion warping can play significant roles in the structural response of composite blades, thus these should be taken into account correctly. Despite vast research activities displayed so far [2-4], as pointed out by Yu [5], there remains still a lack of published results with which to compare for pretwisted composite beams. In other words, there is a strong need to provide benchmark results in the relevant field and also fundamental information on specific subjects inherent in the modeling of pretwisted composite blades.

In general, composite rotor blades are built-up structures made of different materials for the skin and spar and are of closed single- or multi-celled cross-sections. There is a need to properly model the local behavior of the shell wall as a reaction to the global deformation of the blade, even for the thin-walled blade analysis. There have been a few selected research activities to model and analyse thin-walled composite beams with multi-cell sections [6-8]. Mansfield [6] developed a flexibility formulation for thin-walled composite beams with two-cell cylindrical tube section. The equilibrium equations of shell wall are used to derive a [4 × 4] flexibility matrix that captures classical four beam variables (extension, two bendings, and torsion). Chandra and Chopra [7] investigated both analytically and experimentally the structural response of two-cell composite blades with extension-torsion couplings. The stiffness matrix derived is of the order of [9 × 9] since they include derivatives of shear strains as independent variables. Volovoi and Hodges [8] developed closed-form expressions by using the variational-asymptotic beam approach for the stiffness

Presented at the 30th European Rotorcraft Forum, Sept. 14-16, 2004, Marseilles, France.
* Associate Professor, E-mail: snjung@chonbuk.ac.kr
† Graduate Research Assistant

matrics that contain the four classical beam variables. They insisted that shell bending strain measures as well as constraint conditions for each cell of the section were not taken into account consistently in the published literature. Numerical results showing the effects of shell bending strain measures are provided in the paper. Jung, et al. [9] extended the previous mixed beam theory [10] to consider the multi-cell section blades. The theory accounts for the effects of elastic couplings, shell wall thickness, transverse shear couplings, warping, and warping restraint. The theory was applied to composite blades with two-cell airfoil sections. Fairly good correlation with experimental test data has been achieved by using the mixed approach.

Despite vast research efforts devoted so far, the pretwisted composite blades combined with multi-cell sections have not been exploited in the literature. In the present work, the mixed formulation developed in the earlier work [9-10] is extended to cover thin-walled, pretwisted composite blades with multi-cell section. The bending and torsion-related warpings associated with the introduction of pretwist are derived in a closed form in the beam formulation. An extensive validation study with available literature is performed to verify the current approach. The effects of pretwist and fiber orientation angles on the static behavior of thin-walled composite blades are also investigated.

Formulation

Figure 1 shows the geometry and coordinate systems of a pretwisted composite blade with two-cell cross-section. Two different systems of coordinate axes are used: an orthogonal Cartesian coordinate system (*x*, *y*, *z*) for the blade, where *x* is the reference axis of the blade while *y* and *z* are the transverse coordinates of the cross section; a curvilinear coordinate system (*x*, *s*, *n*) for the shell wall of the section, where *s* is the contour coordinate measured along the middle surface of the shell wall and *n* is normal to the contour coordinate. The global deformations of the beam are (*U*, *V*, *W*) along the *x*, *y* and *z* axes, respectively, and ϕ is the twist about the *x*-axis. The local shell deformations are (u, v_t, v_n) along the *x*, *s* and *n* directions, respectively. Allowing the transverse shear deformations, the local deformations at an arbitrary point on the shell wall can be expressed as

$$\begin{aligned} u &= u^0 + n\psi_x \\ v_t &= v_t^0 + n\psi_s \\ v_n &= v_n^0 \end{aligned} \tag{1}$$

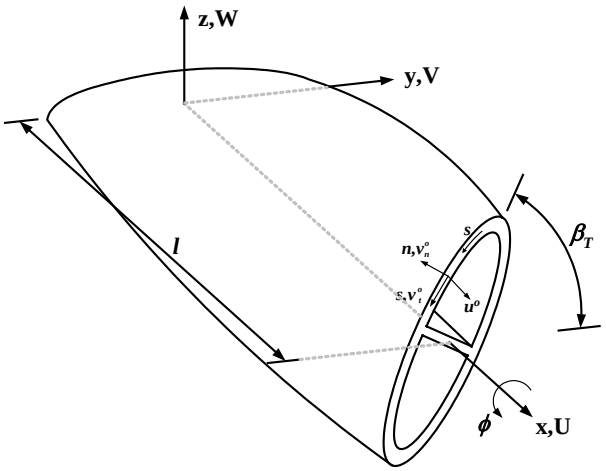

Fig. 1 Geometry and coordinate systems of a pretwisted two-cell blade.

In Eq. (1), u^0, v_t^0 and v_n^0 represent the deformations at the mid-plane of the shell wall and ψ_x, ψ_s represent rotations about the *s*- and *x*-axes, respectively. The shell mid-plane displacements can be obtained in terms of the beam displacements and rotations as follows:

$$\begin{aligned} v_t^0 &= Vy_{,s} + Wz_{,s} + r\phi \\ v_n^0 &= Vz_{,s} - Wy_{,s} - q\phi \\ \psi_s &= \phi \end{aligned} \tag{2}$$

where *r* and *q* are the coordinates of an arbitrary point on the shell wall in the (*n*, *s*) coordinate system, respectively.

Assuming small strains, the strain-displacement relation of the shell wall can be obtained as [10]:

$$\begin{aligned} \gamma_{xs} &= \gamma_{xy}y_{,s} + \gamma_{xz}z_{,s} = u_{,s}^0 + V_{,x}y_{,s} + W_{,x}z_{,s} + r\phi_{,x} \\ \kappa_{xx} &= \beta_{z,x}z_{,s} - \beta_{y,x}y_{,s} + q\phi_{,xx} \\ \kappa_{xs} &= 2\phi_{,x} + \frac{1}{a}(\beta_z y_{,s} + \beta_y z_{,s} - r\phi_{,x}) \end{aligned} \tag{3}$$

where *a* is the local shell radius of curvature and $\overline{\omega}$ is the sectorial area of the section. In Eq. (3), the cross-section rotations β_y and β_z are defined as:

$$\begin{aligned} \beta_y &= \gamma_{xz} - W_{,x} \\ \beta_z &= \gamma_{xy} - V_{,x} \end{aligned} \tag{4}$$

In the above equation, γ_{xy} and γ_{xz} represent the transverse shear strains of the blade in the horizontal and vertical directions, respectively. The strain-displacement relations of Eq. (3) form the basis of the displacement method for thin-walled blades.

Assuming the hoop stress flow N_{ss} in the shell wall is negligibly small, the constitutive relations for the shell wall of the section are written as

$$\begin{Bmatrix} N_{xx} \\ N_{xs} \\ M_{xx} \\ M_{ss} \\ M_{xs} \end{Bmatrix} = \begin{bmatrix} A'_{11} & A'_{16} & B'_{11} & B'_{12} & B'_{16} \\ A'_{16} & A'_{66} & B''_{16} & B'_{26} & B'_{66} \\ B'_{11} & B''_{16} & D'_{11} & D'_{12} & D'_{16} \\ B'_{12} & B'_{26} & D'_{12} & D'_{22} & D'_{26} \\ B'_{16} & B'_{66} & D'_{16} & D'_{26} & D'_{66} \end{bmatrix} \begin{Bmatrix} \varepsilon_{xx} \\ \gamma_{xs} \\ \kappa_{xx} \\ \kappa_{ss} \\ \kappa_{xs} \end{Bmatrix} \tag{5}$$

where the primes over the stiffness constants denote that these are reconstructed using the zero hoop stress flow assumption (N_{ss}=0) from the original A_{ij}, B_{ij} and D_{ij} coefficients appeared in the classical lamination theory [11]. In the present approach, we treat the strain measures ε_{xx}, κ_{xx} and κ_{xs} as the known and derive expressions for the shear flow N_{xs} and the hoop moment M_{ss} in terms of these known quantities by use of the equilibrium equations of the shell wall. It is convenient to write Eq. (5) in a semi-inverted form as:

$$\begin{Bmatrix} N_{xx} \\ M_{xx} \\ M_{xs} \\ \gamma_{xs} \\ \kappa_{ss} \end{Bmatrix} = \begin{bmatrix} C_{n\varepsilon} & C_{n\kappa} & C_{n\phi} & C_{n\gamma} & C_{n\tau} \\ C_{n\kappa} & C_{m\kappa} & C_{m\phi} & C_{m\gamma} & C_{m\tau} \\ C_{n\phi} & C_{m\phi} & C_{\phi\phi} & C_{\phi\gamma} & C_{\phi\tau} \\ -C_{n\gamma} & -C_{m\gamma} & -C_{\phi\gamma} & C_{\gamma\gamma} & C_{\gamma\tau} \\ -C_{n\tau} & -C_{m\tau} & -C_{\phi\tau} & C_{\gamma\tau} & C_{\tau\tau} \end{bmatrix} \begin{Bmatrix} \varepsilon_{xx} \\ \kappa_{xx} \\ \kappa_{xs} \\ N_{xs} \\ M_{ss} \end{Bmatrix} \tag{6}$$

In order to assess the semi-inverted constitutive relations into the beam formulation, a modified form of Reissner's semi-complimentary energy functional Φ_R is introduced:

$$\Phi_R = \frac{1}{2}\begin{Bmatrix} N_{xx}\varepsilon_{xx} + M_{xx}\kappa_{xx} + M_{xs}\kappa_{xs} - \gamma_{xs}N_{xs} \\ -\kappa_{ss}M_{ss} \end{Bmatrix} \tag{7}$$

The stiffness matrix relating beam forces to beam displacements is obtained by using the variational statement of the Reissner functional which is given by [10],

$$\delta \int_0^l \int_C \left\{ \begin{array}{l} \underline{\Phi_R + \gamma_{xs}N_{xs} + \kappa_{ss}M_{ss}} \\ \underline{\underline{+\frac{1}{2}N_{xs}(\gamma_{xs} - u_{,s} - v_{t,x})}} \end{array} \right\} ds dx = 0 \tag{8}$$

(2.8)

where l is the length of the blade. In Eq. (8), the singly underlined terms represent the strain energy density of the blade and the doubly underlined term is the constraint condition with N_{xs} acting as the Lagrange multiplier [8]. Performing the integrals, Eq. (8) results in the equilibrium equations of an element of the shell wall

$$\begin{aligned} &N_{xx,x} + N_{xs,s} = 0 \\ &N_{xs,x} = 0 \\ &M_{xx,x} + M_{xs,s} = 0 \\ &M_{xs,x} + M_{ss,s} = 0 \end{aligned} \tag{9}$$

(2.11a)

as well as the constraint conditions:

$$\begin{aligned} &\gamma_{xs} - u^0_{,s} - v_{t,x} = 0 \\ &\kappa_{ss} - \psi_{s,s} = 0 \end{aligned} \tag{10}$$

The first two equations in Eq. (9) indicate that N_{xs} consists of a constant part and a part that depends on the s-integral of $N_{xx,x}$. In addition, it is found from the third and fourth equations in Eq. (9) that M_{ss} has a constant part, a part that varies linearly with s and a part that depends on the s-integral of $M_{xs,x}$. Hence, one can write

$$\begin{aligned} N_{xs} &= N^0_{xs} - \int_0^s N_{xx,x}\, ds \\ M_{ss} &= M^0_{ss} + yM^y_{ss} + zM^z_{ss} - \int_0^s M_{xs,x}\, ds \end{aligned} \tag{11}$$

where $N^0_{xs}, M^0_{ss}, M^y_{ss}, M^z_{ss}$ represent the circuit shear flows for each of the multi-cell section. For a two-cell blade, specifically, these shear flows and moments lead to eight unknowns that are expressed as:

$$\{n\} = \lfloor n_1 \;\; n_2 \;\; m_1 \;\; m_2 \;\; m_1^y \;\; m_2^y \;\; m_1^z \;\; m_2^z \rfloor^T \tag{12}$$

The continuity condition that must be satisfied for each wall of the section yields the following set of equations [8]:

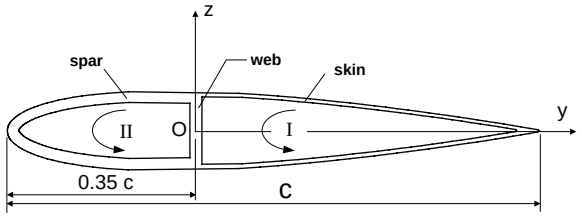

Fig. 2 A two-cell airfoil section.

$$\begin{aligned}
&\oint_I \gamma_{xs} ds = 2A_1\phi_{,x}\,, \qquad \oint_{II} \gamma_{xs} ds = 2A_2\phi_{,x} \\
&\oint_I \kappa_{ss} ds = 0\,, \qquad \oint_{II} \kappa_{ss} ds = 0 \\
&\oint_I y\kappa_{ss} ds = 0\,, \qquad \oint_{II} y\kappa_{ss} ds = 0 \\
&\oint_I z\kappa_{ss} ds = 0\,, \qquad \oint_{II} z\kappa_{ss} ds = 0
\end{aligned} \tag{13}$$

where the subscripts I and II indicate integration over the contour of cells I and II, respectively (see Fig. 2). It is noted that, for a *m*-celled section, the continuity condition results in a set of 4*m* equations. Inserting Eq. (6) into Eq. (13), the unknown shear flows can be obtained as

$$\begin{aligned}
\{n\} &= [Q]^{-1} \cdot \left([P]\{\bar{q}_b\} + [R]\{\bar{q}_{b,x}\} \right) \\
&= [b]\{\bar{q}_b\} + [B]\{\bar{q}_{b,x}\}
\end{aligned} \tag{14}$$

where the derivatives of blade deformations are defined as

$$\{\bar{q}_b\} = \lfloor U_{,x} \;\; \beta_{y,x} \;\; \beta_{z,x} \;\; \phi_{,x} \;\; \phi_{,xx} \rfloor^T \tag{15}$$

In Eq. (14), [*Q*] is a symmetric [8×8] matrix and [*P*] is a fully populated [8×5] matrix. Note that these matrices are integrals over the whole contour and do not contain any coordinates such as *y*, *z* or *s*. Inserting Eq. (14) into Eq. (11), the shear flow and the hoop moment of the section are expressed as

$$\begin{Bmatrix} N_{xs} \\ M_{ss} \end{Bmatrix} = [f]\{\bar{q}_b\} + [F]\{\bar{q}_{b,x}\} \tag{16}$$

It should be noted that the first part of the r.h.s. of Eq. (16) corresponds to the active component of shear flows and the second part corresponds to the reactive component of shear flows according to the terminology adopted in Gjelsvik [12]. The reactive shear flows are dependent on the applied forces and are related with transverse shear degrees of freedom. In order to simplify the analysis, the reactive parts are neglected in the present study. The transverse shear-related couplings can readily be included in a blade where these effects become more important [10].

By using the definition of shear strain γ_{xs} in both the equations (3) and (6), and integrating over 0 to *s*, the displacement field is obtained as

$$u^0 = U + z\beta_y + y\beta_z + \lfloor \psi_i \rfloor \{\bar{q}_b\} \tag{17}$$

where ψ_i denote the cross-section warping distributions that present the following characteristic as

$$\oint \psi_i ds = 0 \tag{17a}$$

Differentiating Eq. (17) with respect to *x*, the axial strain becomes

$$\varepsilon_{xx} = U_{,x} + y\beta_{z,x} + z\beta_{y,x} + \lfloor k\,(y\psi_{i,z} - z\psi_{i,y}) \rfloor \{\bar{q}_b\} \tag{18}$$

where *k* is the initial twist of the blade and is defined as

$$k = \beta_{x,x} \tag{19}$$

where β_x is a rotation of the cross-section about the *x*-axis. In obtaining Eq. (18), the higher order contributions to the axial strain due to the pretwist effect are neglected as the same reason mentioned in Eq. (16).

Inserting Eqs. (6), (16), and (18) into Eq. (8), the strain energy density of a blade results in the beam force-displacement relation as:

$$\{\bar{F}_b\} = \lfloor N \;\; M_y \;\; M_z \;\; T \;\; M_\omega \rfloor^T = [K_{bb}]\{\bar{q}_b\} \tag{20}$$

where *N* is the axial force, M_y and M_z are the bending moments about *y* and *z* directions, respectively, *T* is the twisting moment and M_ω is the Vlasov bi-moment. In the above equation, the [5 × 5] cross-section stiffness matrix $[K_{bb}]$ relates the beam force and moment resultants with beam displacements in an Euler-Bernoulli and Vlasov level of approximation. It should be noted that the higher order parts in Eqs. (16) and (18) along with the doubly underlined term in Eq. (8) contribute to the transverse shear related couplings and this leads to a [7 × 7] stiffness matrix. The details can be found in Ref. 10.

Results and Discussions

Numerical investigation has been performed to correlate the current analysis with available literature and also to identify the influence of pretwist on the structural behavior of composite blades. For the comparison study, various cross-section blades, such as pretwisted metal beams with rectangular solid and single-cell box section, two-celled composite box beams, and two-celled composite blades with extension-torsion couplings, are considered.

Pretwisted metal beams

The first example considered in this study is a pretwisted steel beam used in the work of Durocher and Kane [13]. The length of the beam is 76.2 mm and has a rectangular solid cross-section with 25.4 mm of width and 2.54 mm of thickness. The material properties are: Young's modulus E = 203.4 N/mm^2 and Poisson's ratio ν = 0.3532. The total geometric pretwist angle β_T from root to tip of the beam amounts to 68.8 degrees. The beam is clamped at its root and is loaded at the beam tip. Fig. 3 presents the comparison results of both the axial displacements and induced tip twist for the pretwisted steel beam under the action of tip tension force of 22,250 N. The present results are compared with the analysis results of Durocher and Kane [13] and also with two-dimensional plate/shell finite element analysis results designated in the plot as MSC/NASTRAN 2D. A total of 200 CQUAD4 plate/shell elements are used for the MSC/NASTRAN 2D analysis. As expected, the beam shows an extension-torsion coupled behavior due to the introduction of the geometric pretwist. The agreement between the three different results is seen to be good. In general, the present results with mixed formulation are in a better agreement with the detailed finite element results than those with Durocher and Kane [13]. Fig. 4 shows the comparison of both the tip twist and induced tip tension under a tip torque load of 22.6 N-m. The present predictions are in good agreements with those of Durocher and Kane [13] and MSC/NASTRAN 2D, as is seen in Fig. 4.

The second example is a single-celled, pretwisted box beam studied in Bauchau and Hong [3]. The box beam of span l = 0.635 m has a thin-walled rectangular cross-section (depth 25.4 mm, width 127 mm) with a uniform thickness of 1.07 mm. Young's modulus and shear modulus are E = 115.4 MPa and G = 84.8 MPa, respectively. Fig. 5 shows the comparison of predicted tip twists of the beam with those of Bauchau and Hong

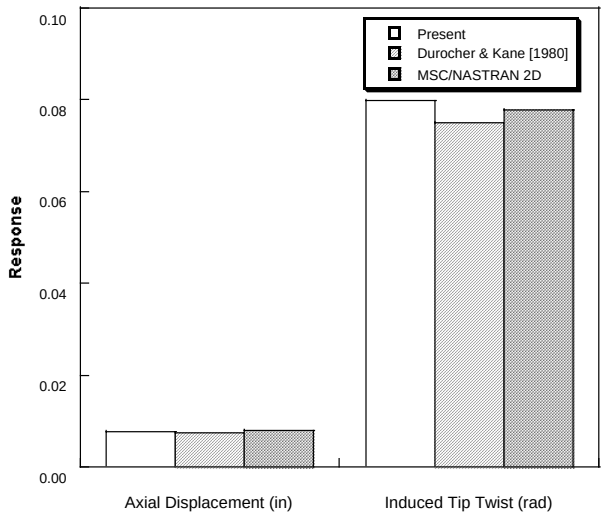

Fig. 3 Comparison of response for pretwisted rectangular solid beam under tip tension (22,250 N).

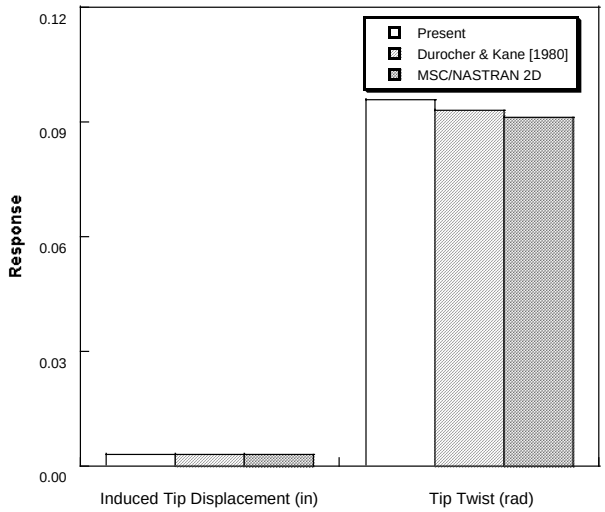

Fig. 4 Comparison of response for pretwisted rectangular solid beam under tip torque (22.6 N-m).

[3] as a function of the pretwist angles. It is seen that the present theory captures clearly both the torsional stiffening under tip torque and the untwisting of the beam under tip tension. Once again, the correlation between the current predictions and the analytical solution by Bauchau and Hong [3] is excellent.

Two-cell composite box-beam

The next example presented is a two-celled, thin-walled composite box-beam with extension-torsion couplings. As described in Fig. 6, the top and bottom walls of the box section are composed of [θ_3/-θ_3] while the vertical walls are composed of [-θ_3/θ_3] such that the extension-

torsion couplings arise. Note that the normal to each wall is directed outward and the order is from top to bottom as is usual in the standard textbook [11]. The positive fiber angles are defined in Fig. 7. The geometry and material properties for the two-cell box beam are summarized in Table 1.

Table 1. Geometry and material properties of two-cell composite box-beams.

Properties	Values
E_{11}	141.9 GPa (20.59 x 10^6 psi)
E_{22}	9.78 GPa (1.42 x 10^6 psi)
G_{12}	6.13 GPa (0.89 x 10^6 psi)
ν_{12}	0.42
Ply thickness, t_p	0.127 mm (0.005 in)
Outer width, 2b	24.21 mm (0.953 in)
Outer depth, 2h	13.64 mm (0.537 in)
Length, l	762 mm (30 in)

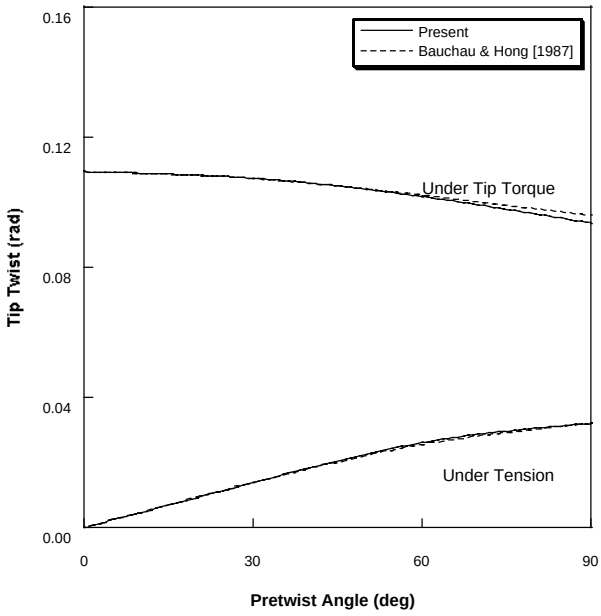

Fig. 5 Comparison of tip twist for pretwisted box beams.

The two-cell box beam depicted in Fig. 6 is studied in Volovoi and Hodges [8]. They presented numerical results showing that the published literature didn't take into account consistently both the shell bending strain measures and constraint conditions for composite beams with multi-cell cross-sections. Fig. 8 shows the comparison of torsion rigidities of two-cell composite box-beams as a function of ply orientation angles. In the plot, the present results are compared with the analytical results by Volovoi and Hodges [8] and with those of two-dimensional MSC/NASTRAN model. A variational-asymptotic beam approach is adopted for the results of Volovoi and Hodges. For the NASTRAN analysis, a finite element mesh composed of 6,600 (150 along the beam span, 44 through the cross-section) CQUAD4 elements is used for the two-celled box-beam. It is seen that there is a clear correlation between the results obtained by three different methods. Though not presented herein, very good correlations are noticed for two-cell box-sections with different layup cases in comparison with the MSC/NASTRAN results. Fig. 9 shows the variation of tip bending slopes as a function of fiber angles for the two-celled box-beam. The present results present a good correlation with the NASTRAN results. The results in Fig. 9 also indicate that the elastic couplings can be quite influential on the beam behavior: the increase of bending slopes obtained at 90 degrees is 13.5 times as high as that at 0 degree. It should be mentioned that this is achieved by purely changing the fiber angles without varying any geometric dimensions of box beams.

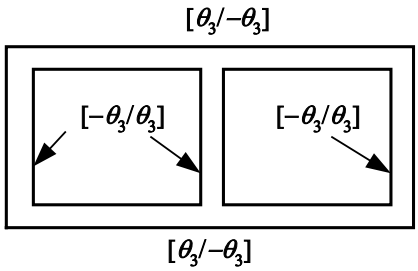

Fig. 6 Extension-torsion coupled layup for two-cell box section.

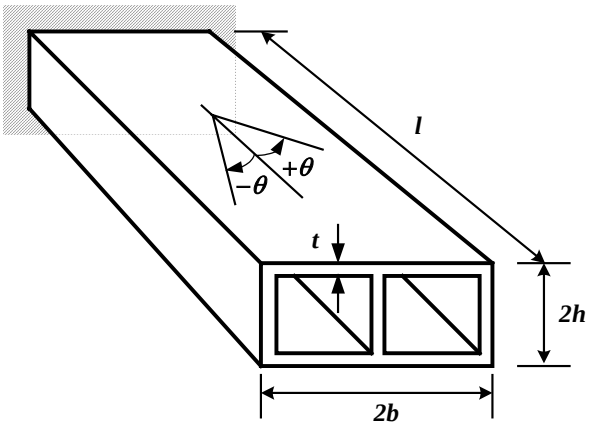

Fig. 7 Schematic of two-cell composite box beam.

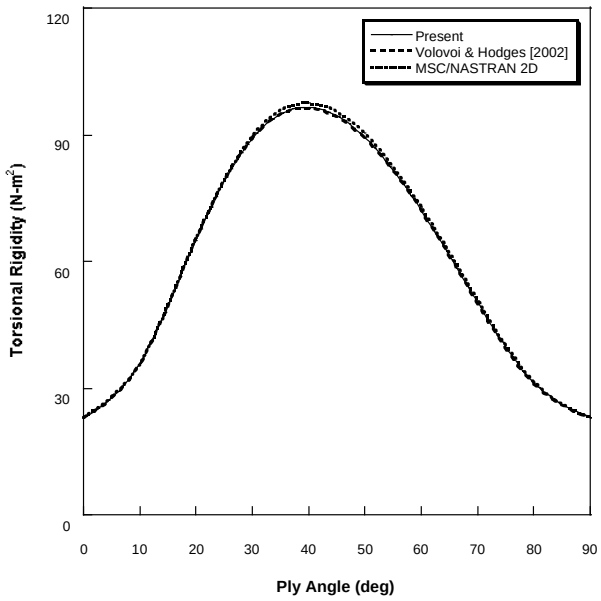

Fig. 8 Comparison of torsional rigidities for two-cell box beams.

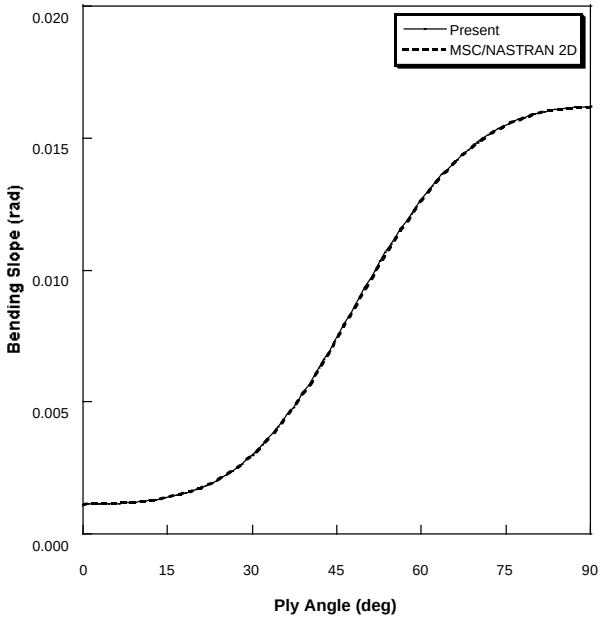

Fig. 9 Comparison of tip bending slopes for two-cell box beams under unit tip shear.

Two-cell composite blades

Numerical simulations are carried out also for coupled composite blades with two-cell airfoil section. Figure 2 shows the schematic of the two-cell blade section that fabricated and tested by Chandra and Chopra [14]. The blade is clamped at one end and warping restrained at both ends. The geometry and the material properties of the blade are given in Table 2. Blades with three different ply layups representing extension-torsion couplings are studied in this section. Note that the bending-torsion coupled blades are already considered in Ref. 9. Table 3 shows the details of the layup used in the blades.

Table 2. Geometry and material properties of composite blades.

Properties	Values
E_{11}	131 GPa (19 x 10^6 psi)
E_{22}	9.3 GPa (1.35 x 10^6 psi)
G_{12}	5.86 GPa (0.85 x 10^6 psi)
ν_{12}	0.40
Ply thickness	0.127 mm (0.005 in)
Airfoil	NACA 0012
Length	641.4 mm (25.25 in)
Chord	76.2 mm (3 in)
Airfoil thickness	9.144 mm (0.36 in)

Figure 10 shows the comparison results of tip bending slopes for the two-cell blades under unit tip shear load. The experimental test data as well as the theoretical results obtained by Chandra and Chopra [14] and with those of the MSC/NASTRAN are compared with the present predictions. For the NASTRAN calculation, a total of 51,600 CQUAD4 plate/shell elements leading 524,131 degrees of freedom are used. As can be seen in the plot, the predictions by the present method are in excellent agreement with experimental results and also with the NASTRAN results and show slightly better correlation than with the analytical results obtained by Chandra and Chopra [14]. It is note that Ref. 14 used a zero-in-plane strain and curvature assumption ($\gamma_{ss}=\kappa_{ss}=0$), while, in the present approach, a zero hoop stress flow assumption ($N_{ss}=0$) is used for the constitutive relations (see Eq. (5)). In addition, the present method adopts a mixed-based approach for the beam formulation, while, in Ref. 14, a classical displacement-based approach is developed. These differences may contribute to the discrepancies as noticed in Fig. 10. Fig. 11 presents the comparison of tip twist response for the three different blades listed in Table 3 under the action of unit tip torque load. A good correlation between the present predictions, experimental results and the two-dimensional MSC/NASTRAN results is clearly seen in the plot. Based on the numerical studies displayed so far, the present beam formulation is thought to capture all the non-classical structural effects of thin-walled composite beams with multi-cell sections in a quite consistent manner.

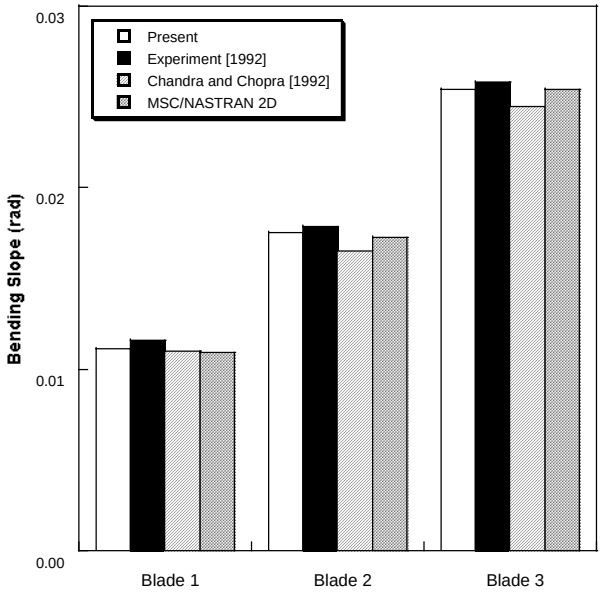

Fig. 10 Comparison of bending slopes for extension-torsion coupled blades under unit tip shear load.

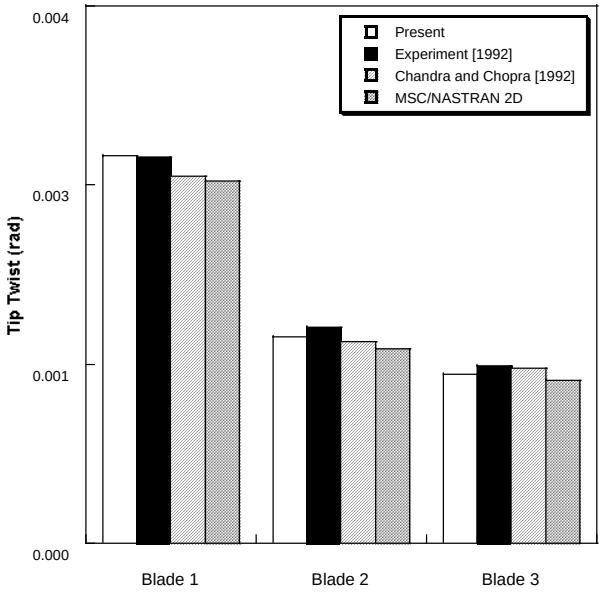

Fig. 11 Comparison of bending slopes for extension-torsion coupled blades under unit tip torque load.

Effect of Pretwist

Finally, the effect of pretwist on the structural response of thin-walled composite box-beam is investigated. For this study, each of the box-beam walls is composed of $[\theta_6]$ to yield an extension-torsion coupling. Fig. 12 shows the normalized tip twist response of $[15_6]$ composite box-beam obtained as a function of pretwist angles. The normalized tip twist is defined as $\phi/\phi|_{\beta_T=0^\circ}$, where $\phi|_{\beta_T=0^\circ}$ is the value of tip twist at zero angle of pretwist. As a means to quantify the pretwist effect on the beam behavior, the slenderness ratio of the box-beam is varied with change of pretwist angles. The slenderness ratio used is the span length divided by the height of the section. The pretwist angle is varied from 0 degree to 90 degrees while the slenderness ratio is decreased from 60 to 5. As expected, the effects of pretwist on the torsional response become larger as the slenderness ratio decreases. As much as 42.8% reduction of tip twist (stiffening) is observed at 90 degrees of pretwist angle and at a slenderness ratio of 5, while the effects seem marginal when the slenderness ratio reaches 60 which falls the usual range of helicopter rotor blades. At this value of slenderness ratio (60), only 3% reduction of twist response is noticed even at 90 degrees of pretwist. The reason seems obvious when we look at the equations (18) and (20): Since the beam stiffness values are influenced by a square of the initial twist *k*, the pretwist affects the structural response in proportion to the square of the pretwist angles while the slenderness ratio is inversely proportional to the square of itself. Thus, blades with low slenderness ratio and high pretwist angles present much larger effect on the torsion behavior.

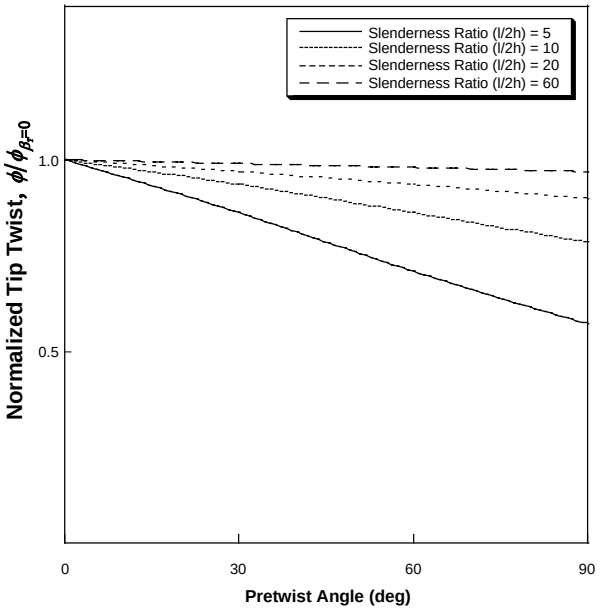

Fig. 12 Effect of slenderness ratios on the twist response of pretwisted composite box beam.

As mentioned before, the results in Fig. 12 are obtained when the fiber angles held fixed ($\theta = 15^o$). In Fig. 13, the effects of fiber angles on the torsion response of

pretwisted box-beams are investigated with varying the pretwist angles. In this case, the fiber angles in the box-beam walls are varied in the positive or negative direction while the slenderness ratio is held fixed to 20. It is seen that both the fiber angles and pretwist angles affect the torsional behavior of the beam significantly. The maximum change occurs at 15 degrees of fiber angles. The amount of increase reaches 6.6% at the positive 15 degrees, and as much as 10.1% reduction in twist angle is noticed at the negative 15 degrees. Note that the positive fiber angles have a softening effect while the negative angles present a stiffening effect on the torsion response. This result indicates that obtaining an appropriate combination of composite fiber angles and pretwist angles needs thorough investigation for optimum rotors.

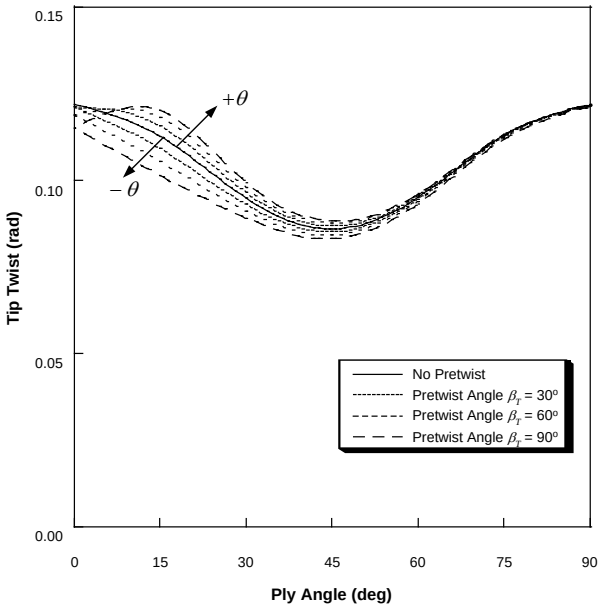

Fig. 13 Effect of fiber orientation angles on the twist response of pretwisted composite box beam.

Concluding Remarks

In the present work, a mixed beam formulation for thin-walled pretwisted composite blades with multiple-cell sections has been developed. The beam force-displacement relations of the blade are obtained by using the Reissner's semi-complementary energy functional. The bending and torsion-related warpings introduced with the pretwist effect are derived in a closed form in the beam formulation. The theory has been validated with available literature and detailed finite element results for coupled composite beams and blades with various cross sections. These include pretwisted beams with rectangular solid and single-cell box-section, composite beams with two-cell box section, and two-cell composite blades. Good correlation of responses with other literature is obtained for all the test cases considered. The effects of pretwist and fiber orientation angles on the static behavior of thin-walled composite box beam are also investigated. It is shown that the pretwist effects become pronounced at beams with low slenderness ratios. For $[15_6]$ composite box-beam case, the reduction of tip twist amounts to 42.8% at 90 degrees of pretwist angle and at a slenderness ratio of 5. In addition, the positive fiber angles have a softening effect while the negative angles present a stiffening effect on the torsion response. The amount of increase reaches 6.6% at the positive 15 degree case, and as much as 10.1% reduction in twist angle is noticed at the negative 15 degree case.

Acknowledgement

This research was performed for the Smart UAV Development program, one of 21st Century Frontier R&D Programs funded by the Ministry of Science and Technology of Korea.

References

1. Rosen, A., "Structural and Dynamic Behavior of Pretwisted Rods and Beams," *Applied Mechanics Review*, Vol. 44, No. 12, Part 1, Dec. 1991, pp. 483-515.
2. Cesnik, C. E. S., Hodges, D., and Sutyrin, V. G., "Cross-sectional Analysis of Composite Beams Including Large Initial Twist and Curvature Effects," *AIAA Journal*, Vol. 34, No. 9, Sept. 1996, pp. 1913-1920.
3. Bauchau, O. A., and Hong, C. H., "Large Displacement Analysis of Naturally Curved and Twisted Composite Beams," *AIAA Journal*, Vol. 25, No. 11, Nov. 1987, pp. 1469-1475.
4. Pai, P. F., and Nayfeh, A. H., "A Fully Nonlinear Theory of Curved and Twisted Composite Rotor Blades Accounting for Warping and Three-Dimensional Stress Effects," *Int. Journal of Solids and Structures*, Vol. 9, 1994, pp. 1309-1340.
5. Yu, W., "Variational Asymptotic Modeling of Composite Dimensionally Reducible Structures," *Ph.D Thesis*, Georgia Institute of Technology, July 2002.
6. Mansfield, E. H., "The Stiffness of a Two-Cell Anisotropic Tube," *Aeronautical Quarterly*, May 1981, pp. 338-353.
7. Chandra, R., and Chopra, I., "Structural Behavior of Two-Cell Composite Rotor Blades with Elastic

Couplings," *AIAA Journal*, Vol. 30, No. 12, Dec. 1992, pp. 2914-2921.
8. Volovoi, V. V., and Hodges, D. H., "Single- and Multi-Celled Composite Thin-Walled Beams," *AIAA Journal*, Vol. 40, No. 5, May 2002, pp. 960-965.
9. Jung, S. N., and Nagaraj, V. T., "Structural Behavior of Thin- and Thick-Walled Composite Blades with Multi-Cell Sections," *Proceedings of the 43rd Structures, Structural Dynamics, and Materials Conference*, Denver, CO, Apr. 22-25, 2002, AIAA-2002-1432.
10. Jung, S. N., Nagaraj, V. T., and Chopra, I., "Refined Structural Model for Thin- and Thick-Walled Composite Rotor Blades," *AIAA Journal*, Vol. 40, No. 1, Jan. 2002, pp. 105-116.
11. Jones, R. M., *Mechanics of Composite Materials*, McGraw-Hill Book Co., N.Y., 1975.
12. Gjelsvik, A., *The Theory of Thin Walled Bars*, John Wiley & Sons, Inc., 1981.
13. Durocher, L. L., and Kane, J., "A Preliminary Design Tool for Pretwisted, Tapered Beams for Turbine Blades," *Transactions of ASME, Journal of Mechanical Design*, Vol. 102, Oct. 1980, pp. 742-748.
14. Chandra, R., and Chopra, I., "Structural Response of Composite Beams and Blades with Elastic Couplings," *Composites Engineering*, Vol. 2, Nos. 5-7, 1992, pp. 347-374.
15. Chandra, R., and Chopra, I., "Coupled Composite Rotor Blades under Bending and Torsional Loads," *AHS Specialists' Meeting on Rotorcraft Structures*, Williamsburg, Virginia, Oct. 28-31, 1991.

Table 3. Lay-up cases of two-cell composite blades.

Cases	Spar		Web	Skin
	Top Flange	Bottom Flange		
Blade 1	$[0/15]_2$	$[0/15]_2$	$[0/15]_2$	[15/-15]
Blade 2	$[0/30]_2$	$[0/30]_2$	$[0/30]_2$	[30/-30]
Blade 3	$[0/45]_2$	$[0/45]_2$	$[0/45]_2$	[45/-45]